Simulation of wave propagation in weakly cohesive powders by discrete element method

A. Buklakov, Jean-Noël Roux, F. Grekova

Simulation of wave propagation in weakly cohesive powders by DEM

Buklakov E.A.,
Peter the Great Saint-Petersburg Polytechnic University, Russia; e-mail: buklakovegor@mail.ru
Roux J.-N.
Laboratoire Navier, Université Gustave Eiffel; e-mail: jean-noel.roux@univ-eiffel.fr
Grekova E.F.
Institute for Problems in Mechanical Engineering RAS; e-mail: elgreco@pdmi.ras.ru

The propagation of elastic plane waves in a 2D model of a weakly cohesive powder is numerically simulated by the discrete element method (DEM). Isotropic samples of disks interacting by elasticity, friction and cohesion in their contacts are first assembled in equilibrium states under isotropic pressure. Contact laws are linearized in elastic form, with fixed normal (K_N) and tangential (K_T) stiffness constants, to model the reponse to a sine-shaped impulse (main frequency ω) imparted to the sample boundary. The shape of this disturbance depends on the value of ω, relative to basic frequency $\omega^* \equiv \sqrt{K_N/m}$ (m denoting the grain mass). Longitudinal and transverse waves triggered at low ω/ω^* propagate with a coherent wavefront followed by an incoherent tail, with the classical velocity deduced from static moduli. Higher values of ω/ω^* result in much smaller coherent signals and a strong localization of the energy near the source. Longitudinal waves are accompanied by disordered rotations, travelling with another velocity, induced at all times during propagation. Transverse waves contain both rotational and translational components. It is speculated that reduced Cosserat theories could be relevant for such materials on the continuum scale.

1 Introduction

While the application of discrete element modeling (DEM) to granular materials is now widespread, the control of a reproducible packing states, and the characterization of their microstructure are still being studied. *Cohesive* materials exhibit a considerably wider variety of internal structures, and therefore open a larger field of investigation. Examples of such materials include powders used in copying equipments, fine flour, wet sand, and large classes of colloidal aggregates. The propagation of small amplitude elastic waves, as in the experiments of Refs. [1, 2] is an interesting method to probe their microstructure-dependent mechanical properties. The dispersion observed in these experiments, apparently, cannot be described in terms of classical dissipative continua. One of the possibilities is that some other degrees of freedom influence the powder dynamics, leading to an "optical branch". DEM simulations of wave propagation in disordered packings [6, 7] are also relatively scarce.

The DEM-based study, which the present publication reports on, is still at a rather early stage. We address the issue of the nature of wave propagation (dealt with in s Sec. 3)and its relation to material properties, in a deliberately simplified two-dimensional (2D) model of a cohesive power. The DEM ingredients and the sample preparation (as briefly presented in Sec. 2) are the same as used in Refs. [3, 4]. Although the present report deals with rather dense states, it is planned to investigate the loose structures, akin to colloidal gels, observed in those references.

2 Discrete model

2.1 DEM parameters

All simulations are carried out in the absence of gravity. The model material is an assembly of disks, with a uniform distribution of diameters between $d_{\min}$ and $d_{\max} = 2d_{\min}$, the latter being chosen as the unit of length, while its mass m is the unit of mass (the 2D mass density in the disks is thus equal to $4/\pi$). The model material and the DEM ingredients are the same as in Ref. [3], which may be consulted for more details. Contacting disks are pressed against each other by (radius-independent) adhesive force F_0, set to 1. Contact deflection is opposed by a repulsive elastic force F_n^e computed with (radius-independent) normal stiffness K_n, while sliding relative displacements give rise to a tangential elastic force F_t involving stiffness K_t (we choose $K_t = K_n$). The adopted value $K_n = 10^5 F_0/d_{\max}$ ensures that contact de-

flections remain very small. The Coulomb condition, $|F_t| \leq \mu F_n^e$, applies with friction coefficient $\mu = 0.3$. In the assembling dynamical stage, some viscous dissipation is also introduced (we discard it on simulating elastic waves). The characteristic frequency defined in the abstract, using the largest grain mass, is thus $\omega^* = \sqrt{K_n} = 10^{5/2}$ in the chosen units. We also use notation $t_0 = 1/\omega^*$.

2.2 Packing procedure

Rectangular samples (as shown in Fig. 1) with aspect ratio close to 2 are prepared under isotropic pressure P by the procedure of. Ref. [3], which we very quickly summarize here. First, the grains,

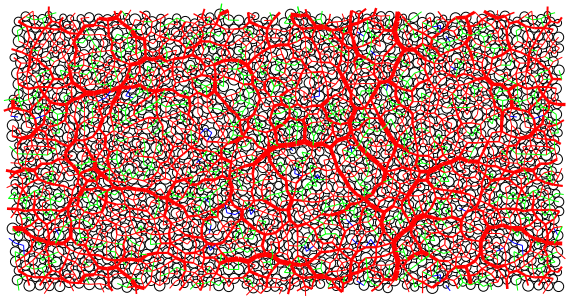

Figure 1: Rectangular isotropic sample of 6300 grains, in equilibrium under $P^* = 1$. Normal force intensity encoded as line thickness, sign as colour: red = compressive, green = tensile, blue = 0.

randomly placed in a periodic cell at low density, are assembled by ballistic aggregation, with random initial velocities and dissipative collisions. Once a static loose structure connecting all grains, stuck together by the adhesive force, it is quasistatically compressed at growing pressure P, reducing the cell size and increasing solid fraction Φ. This process is governed by dimensionless reduced pressure $P^* = Pd_{\max}/F_0$. Here we first study the rather dense states (Fig. 1) obtained at $P^* = 1$. The samples have solid fraction $\Phi \simeq 0.80$ and coordination number $\zeta \simeq 3.5$. Compared to Ref. [6], dealing with a maximally dense and highly coordinated state, the material states we investigate are more appropriate for (preconsolidated) cohesive granular assemblies. The longitudinal elastic modulus $C_{11} = \lambda + 2\mu = 0.46 \pm 0.02 K_N$ (λ being the Lamé coefficient), and the shear modulus, $\mu \simeq 0.16 K_N$ are measured as in Ref. [4]. The elastic stiffness responsible for the resistance to the rotation of the grain relatively to its neighbourhood is known as the Cosserat couple modulus in the micropolar theory. We measure it as a coefficient of proportionality of an applied uniform body moment to mass-averaged particle rotation (note that the macroscopic displacement gradient vanishes due to periodic boundary conditions in a fixed cell), with value $\alpha = 0.158 K_N$. We also calculate another specific frequency (in micropolar continuum it will be an approximation for the cut-off frequency) $\omega_0 = 4.7\omega_*$. This is the frequency of free rotational oscillations, when all the particles are initially given the same angular displacement.

2.3 Wave propagation: methods

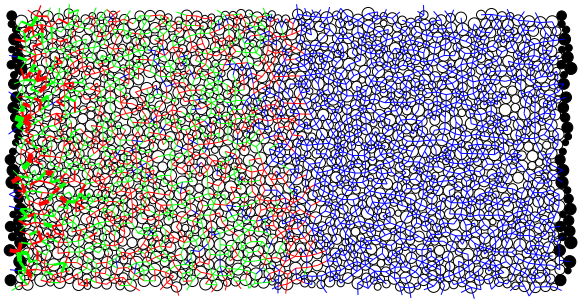

Figure 2: Wave propagation through the sample. Wall grains in black. Codes of Fig. 1 now apply to force *increments*.

To simulate the propagation of a wave along the sample length (along the axis of coordinate x), we first replace periodic conditions in direction x by a pair of walls, made of grains moving together like a single rigid body. Computations are carried out on linearizing the force laws for small increments about the initial prestressed state described above. We assume that the contact network does not change, and that all contact forces remain in the elastic regime (no frictional sliding). Constants K_n, K_t and grain inertia are the only parameters in the computations. Specifically, the elastic force increment $\mathbf{F}^e_{ji}$ between grains i and j of radii $R_{i,j}$, relates to their displacements $\mathbf{u}_{i,j}$ and rotations $\theta_{i,j}$ in their contact, $\mathbf{n}_{ij}$ and $\mathbf{t}_{ij}$ denoting the normal and tangential unit vectors, reads

$$\mathbf{F}^e_{ji} = K_n \left[(\mathbf{u}_j - \mathbf{u}_i) \cdot \mathbf{n}_{ij}\right] \mathbf{n}_{ij} + K_t \left[(\mathbf{u}_j - \mathbf{u}_i) \cdot \mathbf{t}_{ij} - (R_j\theta_j + R_i\theta_i)\right] \mathbf{t}_{ij}. \quad (1)$$

Masses m_i and moments of inertia I_i enter the

equations of motion,

$$m_i\ddot{\mathbf{u}}_i = \sum_j \mathbf{F}^e_{ji}, \qquad I_i\ddot{\theta}_i = \sum_j R_i\mathbf{n}_{ij} \times \mathbf{F}^e_{ji}. \quad (2)$$

We apply a sine-shaped impulse (only one period long) with frequency ω at the left wall, which is requested to move in direction x (longitudinal wave) or y (transverse wave). We restrict our attention to times for which the wave front has not reached the fixed right wall (Fig. 2). Displacements, rotations and energy are averaged in slices parallel to transverse direction y with width $d_{\max}$.

3 Wave propagation: results

3.1 Longitudinal wave

At low frequencies a longitudinal perturbation behaves as a travelling decaying wave (Fig. 3), but at

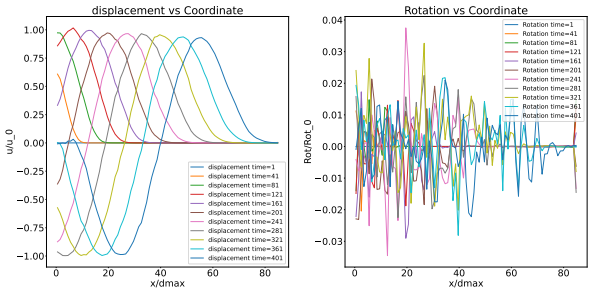

Figure 3: Longitudinal wave. Displacements (left) and rotations (right) at frequency $0.05\omega^*$ vs. x. Different graphs correspond to different times.

high frequencies it either moves at a very slow velocity, or stays localized near the left wall (Fig. 4). We also observe disordered incoherent rotational

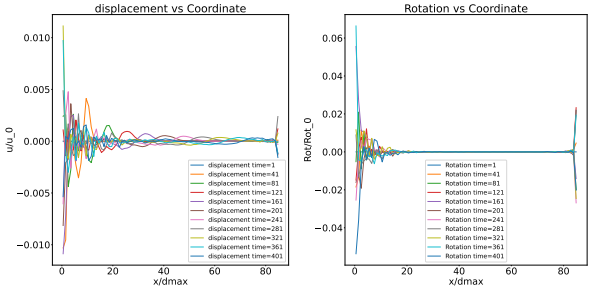

Figure 4: Longitudinal wave. Displacements (left) and rotations (right) at frequency $8\omega^*$ vs. x. Different graphs for different times.

perturbations, which at the same velocity as displacements, for different frequencies. Apparently, these rotational perturbations are produced in the focii of local anisotropy, heterogeneously oriented and distributed in the sample. In these focii the wave becomes mixed. In the simplest model of the homogeneous anisotropic reduced Cosserat medium this coupling grows with frequency, until it reaches a certain threshold of the order of ω_0 [5]. Here we also observe that rotations are more present at larger frequencies. However, this continuum model cannot be directly applied to our case, since our sample is locally anisotropic. The propagation of energy at low and high frequencies looks similar (Fig. 5).

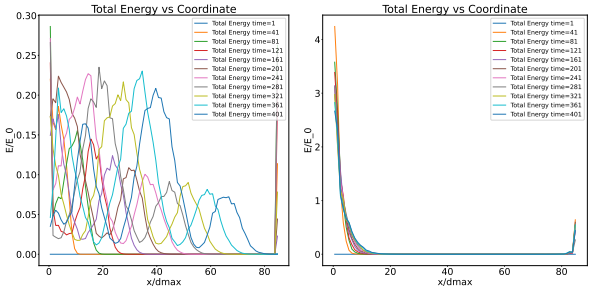

Figure 5: Longitudinal wave. Energy at a frequency $0.05\omega^*$ (left, travelling) and $8\omega^*$ (right, localized near the wall) vs coordinate x. Different graphs for different times.

3.2 Transverse wave

For the transverse wave, unlike in the previous case, displacements and coherent rotations move at the same velocity but with a phase shift of $\pi/2$ (Fig. 6), i.e. the transverse wave has both translational and rotational componnents. This is characteristic for isotropic Cosserat media. At high frequencies the transverse wave, as well as the longitudinal one, is also localized near the wall (or moves at a very slow velocity), see Fig. 7. We see that only a small part of the total energy travels at low frequencies, the larger part staying in the vicinity of the left wall, even as some perturbations arrive at the right wall (Fig. 8). We see the evolution of the energy distribution in the sample for different frequencies in (Figs. 9–12). Comparison of the fraction of energy, contained in the left 1/8 part of the sample, as a function of time, is shown in Fig. 13 for different frequencies. Note that these very slow or localized waves are observed below the cut-off frequency ω_0,

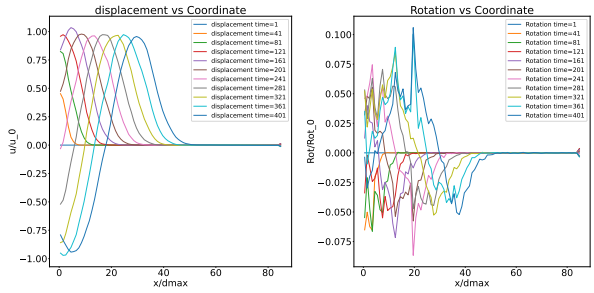

Figure 6: Transverse waves. Displacements (left) and rotations (right) vs x, at frequency $0.05\omega^*$. Different graphs for different times.

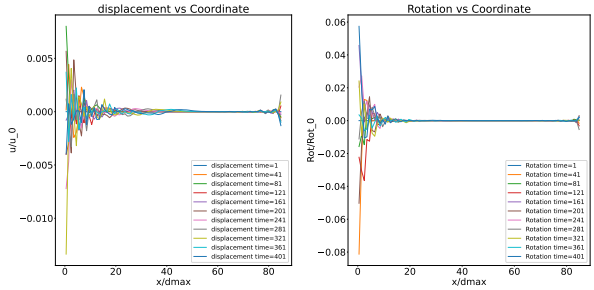

Figure 7: Displacements (left) and rotations (right) at frequency $8\omega^*$, versus x in transverse wave. Different lines for different times.

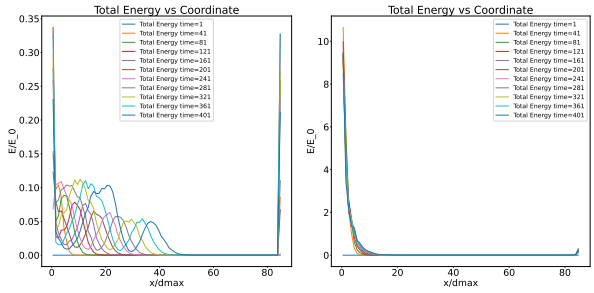

Figure 8: Transverse wave, $\omega = 0.05\omega^*$ (left) and $8\omega^*$ (right). Energy vs x-coordinate. Different graphs for different times.

which corresponds to one of eigen modes of the discrete system. Therefore it is not related to the discrete structure of the medium, which does not react to a too short impulse. This phenomenon is typical for the reduced Cosserat medium. However, in an isotropic reduced Cosserat medium there is no such effect for a longitudinal wave, which we have in our experiment.

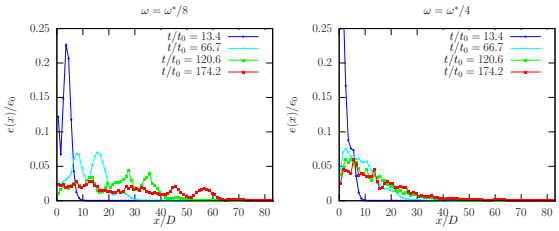

Figure 9: Transverse wave at relatively low frequencies. Energy vs x-coordinate at different times.

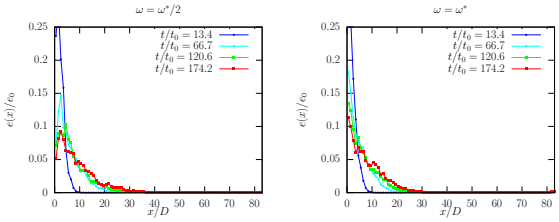

Figure 10: Transverse wave at intermediate frequencies. Energy vs. x-coordinate at different times.

3.3 Wave velocity

If we measure by the time of flight method the velocity of displacement waves, e.g. register the first signal arriving to the given co-ordinate, and calculate the speed as the slope of the distance versus time curve, we obtain that displacements travel with the same velocity independently of the frequency of the sinusoidal impulse we send (Fig. 14). This seems to be in contradiction with the highly dispersive character if the waves at high frequencies. The reason of this behaviour is, apparently, the following: we induce various frequencies (or excite various eigenmodes of the discrete system) by a sinusoidal impulse, and register those that arrive first. They do not necessary correspond to the fre-

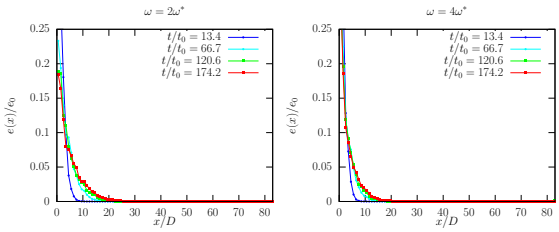

Figure 11: Transverse wave at high frequencies. Energy vs x-coordinate at different times.

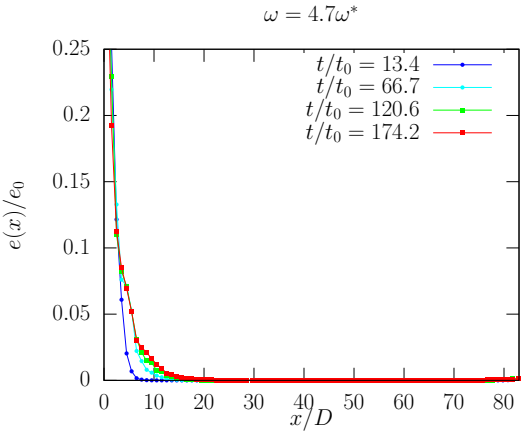

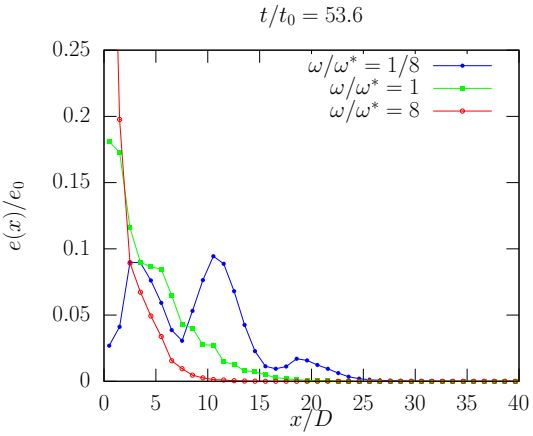

Figure 12: Transverse wave at the cut-off frequency and comparison of energy propagation at the same moment of time for different frequencies.

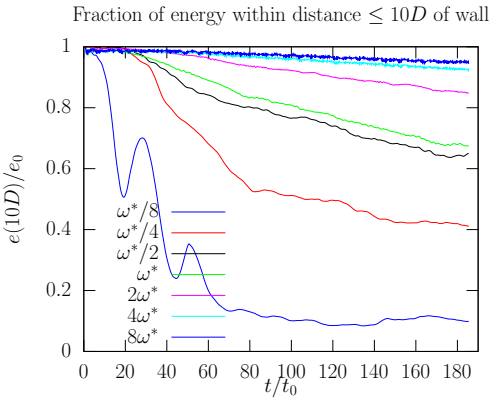

Figure 13: Transverse wave. Fraction of total energy within distance $10d_{\max}$ of left wall versus time, for different frequencies. At low ω energy travels, at high ω it stays localized near the wall.

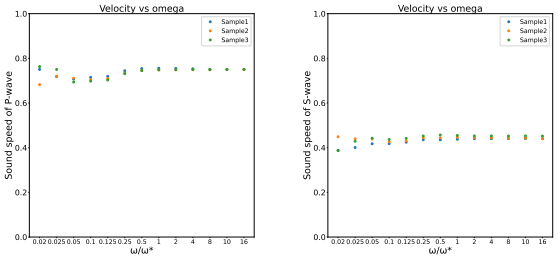

Figure 14: Displacement wave velocity, normalized by $d_{\max}\omega^*$, versus frequency for longitudinal (left) and transverse (right) waves.

quency of the impulse.

The same procedure for the energy gives us a different picture for the longitudinal and transverse waves (Fig. 15). Here we see a jump in velocity near $\omega_*/4$ for transverse waves and near ω_* for longitudinal waves. Then the energy propagates very slowly (as we have seen it in the previous section). This is not completely clear if this corresponds to the optical branch, or localization in the band gap that reduced continua have, or, perhaps, some effect of the scattering by heterogeneities, resulting in the effective dissipation.

These data are compared to the longitudinal (C_p) and transverse (C_s) low frequency wave velocities deduced from the static moduli:

$$C_p = \sqrt{(\lambda + 2\mu)/\rho}, \quad C_s = \sqrt{\mu/\rho} \qquad (3)$$

ρ being the mass density of the medium. In our

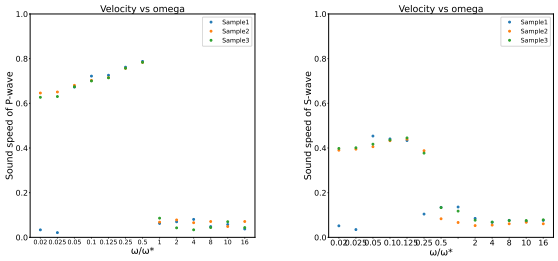

Figure 15: Energy propagation for the longitudinal (left) and transverse (right) waves. Wave velocity, normalized by $d_{\max}\omega^*$, versus frequency.

system, formulae (3) yield $C_p = 0.640\, d_{\max}\omega^*$ and $C_s = 0.385\, d_{\max}\omega^*$, in very good agreement with the observations at low frequency.

Conclusion

We prepare in a reproducible way a 2D packing imitating isotropic and slightly heterogeneous sample of a weakly cohesive powder made from elastic spherical particles with varying radii. We investigate linear waves near a nonlinear equilibrium in such samples. Both longitudinal and transverse waves at high frequencies are strongly attenuated and slow or do not propagate. A transverse wave is a shear-rotational wave: the rotations propagate at the same speed, the phase difference is $\pi/2$. It is possible that reduced models, analogous to reduced Cosserat models, are appropriate for description of this medium. However, they need a modification, since the longitudinal wave is purely translational, but at all times causes incoherent rotations, propagating at a different speed and taking part of the energy of the longitudinal wave. This is probably due to heterogeneously oriented and distributed focii of local anisotropy. The transverse wave is more sensitive to the specific realization of the sample than the longitudinal one. The rotational perturbation accompanying it, on the contrary, is more coherent for a transverse wave than for a longitudinal one.

References

[1] Botello, F. R., Castellanos, A., and Tournat, V. (2016). Ultrasonic probing of cohesive granular media at very low consolidation. *Ultrasonics*, 69:193–200.

[2] Botello, F. R., Quintanilla, M. A., Castellanos, A., Grekova, E. F., and Tournat, V. (2018). Effect of the microstructure on the propagation velocity of ultrasound in magnetic powders. *Ultrasonics*, 82:153–160.

[3] Gilabert, F., Roux, J.-N., and Castellanos, A. (2007). Computer simulation of model cohesive powders: Influence of assembling procedure and contact laws on low consolidation states. *Physical Review E*, **75**(1):011303.

[4] Gilabert, F., Roux, J.-N., and Castellanos, A. (2008). Computer simulation of model cohesive powders: Plastic consolidation, structural changes, and elasticity under isotropic loads. *Physical Review E*, **78**(3):031305.

[5] Grekova, E.F. (2016). Plane waves in the linear elastic reduced Cosserat medium with a finite axially symmetric coupling between volumetric and rotational strains. *Mathematics and Mechanics of Solids*, **21**(1):73–93.

[6] Saitoh, K., Shrivastava, R. K., and Luding, S. (2019). Rotational sound in disordered granular materials. *Physical Review E*, **99**(1):012906.

[7] Somfai, E., Roux, J.-N., Snoeijer, J. H., Van Hecke, M., and Van Saarloos, W. (2005). Elastic wave propagation in confined granular systems. *Physical Review E*, **72**(2):021301.